2011 International Conference on Electrical Engineering and Informatics
17-19 July 2011, Bandung, Indonesia

A Novel Control Technique for Single-Phase Grid-Connected Inverters

S. Golestan[#1], *Member, IEEE*, M. Monfared[*2], *Member, IEEE*, and J. M. Guerrero[&3], *Senior Member, IEEE*

[#]*Department of Electrical Engineering, Abadan Branch, Islamic Azad University*
Abadan 63178-36531, Iran
[1]s.golestan@ieee.org
[*]*Department of Electrical Engineering, Ferdowsi University of Mashhad*
Mashhad 91775-1111, Iran
[2]m.monfared@ieee.org
[&]*Department of Automatic Control Systems Computer Engineering Universitat Politècnica de Catalunya*
Comte d'Urgell 187. 08036 Barcelona. Spain
[3]josep.m.guerrero@upc.edu

***Abstract*—A synchronous reference frame controller with a multi-resonant harmonic compensator for single-phase grid-connected inverters is proposed in this paper. The essence of the proposed control strategy is to use a synchronous reference frame PI controller (SRFPI) to regulate the output current with zero steady state error, together with a multi-resonant harmonic compensator to provide an efficient attenuation of the grid voltage background harmonic distortion, and an average power controller to regulate the active and reactive powers. A detailed design procedure for the proposed control strategy is presented based on a frequency response approach. Extensive simulations confirm the validity of the proposed strategy.**

I. Introduction

Generally, the DG systems can operate either in islanding mode or in grid-connected mode, and this paper focuses on the latter. The single-phase current-controlled voltage source inverters (CC-VSI) are commonly used to provide the interface between small DG systems and the utility grid.

Various researches on control of the single-phase inverters in grid-connected mode have been presented in literature [1], [2], and [3], among which, the PI-type ramp comparison controller with grid voltage feed-forward has a long history of use due to its simplicity and robustness [3]. This simple control technique, however, has two main drawbacks: inability to track a sinusoidal command with zero steady-state error due to the limited gain at the fundamental frequency and poor disturbance rejection capability.

To overcome the aforementioned drawbacks, a SRFPI controller plus a multi-resonant harmonic compensator is proposed in this paper. The essence of the proposed control strategy is to use a SRFPI to regulate the output current with zero steady state error, together with a multi-resonant harmonic compensator to provide an efficient attenuation of the grid voltage background harmonic distortion, and an average power controller to regulate the active and reactive power injection into the grid. The operation principle of the proposed control strategy is explained in details, and, simulation results are reported, to confirm the effectiveness of this control technique.

II. SRFPI Controller for Single-Phase Inverters

SRFPI controllers are commonly used in three-phase systems and operate by transforming the three-phase ac signals into DC components in the synchronously rotating frame so that the steady-state error that is normally associated with the application of PI control to ac signals can be eliminated. Unfortunately, these controllers are not applicable to single-phase converters, where there is only one phase available, while the DQ transformation requires a minimum of two orthogonal signals. In order to create the required orthogonal phase information from the original single-phase signal, different methods can be utilized [4]. In this paper, we use a first-order all-pass filter (APF), as shown in equation (1), to create the required orthogonal signal.

$$APF = \frac{\omega - s}{\omega + s} \tag{1}$$

where ω is the fundamental frequency.

The DQ transformation can be implemented once the required orthogonal signal is generated. Equation (2) defines the transformation from stationary ($\alpha\beta$) to rotating (DQ) reference frame, and equation (3) defines the reverse transformation.

$$T = \begin{bmatrix} cos(\omega t) & sin(\omega t) \\ -sin(\omega t) & cos(\omega t) \end{bmatrix} \tag{2}$$

$$T^{-1} = \begin{bmatrix} cos(\omega t) & -sin(\omega t) \\ sin(\omega t) & cos(\omega t) \end{bmatrix} \tag{3}$$

III. System Modeling

Fig. 1 shows the converter system considered in this investigation. Salient parameters for the system are shown in Table I.

The bilinear differential equations that describe the large-signal dynamic behavior of this converter are as follows:

$$uV_{dc} = v_C + L_1 \frac{di_L}{dt} + r_1 i_L \tag{4}$$

$$v_C = v_g + (L_2 + L_g)\frac{di_o}{dt} + (r_2 + r_g)i_o \tag{5}$$

978-1-4577-0751-3/11/$26.00 ©2011 IEEE

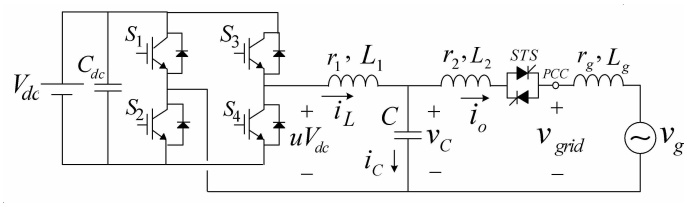

Fig. 1. Single-phase grid-connected inverter

TABLE I
SYSTEM PARAMETERS

Symbol	Quantity	Value
P_o	Rated output power	$2.5\,kW$
f_s	Switching frequency	$18\,kHz$
V_{dc}	Dc-link voltage	$300\,V$
L_1	LCL-filter inverter-side inductance	$1.5\,mH$
r_1	LCL-filter inverter-side parasitic resistance	$0.1\,\Omega$
C	LCL-filter Capacitance	$7\,\mu F$
L_2	LCL-filter grid-side inductance	$1.5\,mH$
r_2	LCL-filter grid-side parasitic resistance	$0.1\,\Omega$
v_g	Nominal grid voltage (rms)	$120\,V$
$L_{g\,s}$	Grid inductance at stiff grid situation	$100\,\mu H$
$r_{g\,s}$	Grid resistance at stiff grid situation	$0.1\,\Omega$
$L_{g\,w}$	Grid inductance at weak grid situation	$3.3\,mH$
$r_{g\,w}$	Grid resistance at weak grid situation	$1.5\,\Omega$

$$C\frac{dv_C}{dt} = i_C = i_L - i_o \tag{6}$$

where, u is the control variable.

Assuming that the switching frequency is high enough to neglect the inverter dynamics, a block diagram of the equivalent circuit based on (4)-(6) may be constructed as shown in Fig. 2, where, $d(s)$ denotes the duty cycle of the inverter.

From Fig. 2, the inverter output current i_L can be written as:

$$i_L = G_1(s)d(s) - G_2(s)v_g(s) \tag{7}$$

where:

$$G_1(s) = \frac{(L_2+L_g)Cs^2 + (r_2+r_g)Cs + 1}{d_3s^3 + d_2s^2 + d_1s + d_0}V_{dc} \tag{8}$$

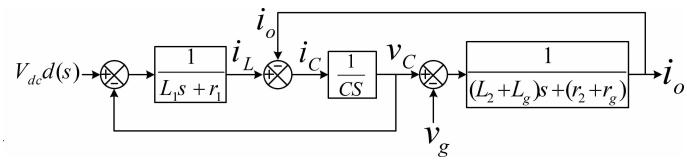

Fig. 2. Block diagram of single-phase grid-connected inverter

$$G_2(s) = \frac{1}{d_3s^3 + d_2s^2 + d_1s + d_0} \tag{9}$$

The coefficients d_3, d_2, d_1, and d_0 can be expressed as:

$$d_3 = L_1C(L_2+L_g) \tag{10}$$

$$d_2 = [(r_2+r_g)L_1 + r_1(L_2+L_g)]\,C \tag{11}$$

$$d_1 = L_1 + L_2 + L_g + r_1(r_2+r_g)C \tag{12}$$

$$d_0 = r_1 + r_2 + r_g \tag{13}$$

IV. PROPOSED CONTROL STRATEGY

The essence of the proposed control strategy, as shown in Fig. 3, is to use a SRFPI controller to regulate the inductor current i_L, together with a multi-resonant harmonic compensator to provide an efficient attenuation of the grid voltage background harmonic distortion, and an average power controller to generate references $i^*_{L,dq}$ for the current controller.

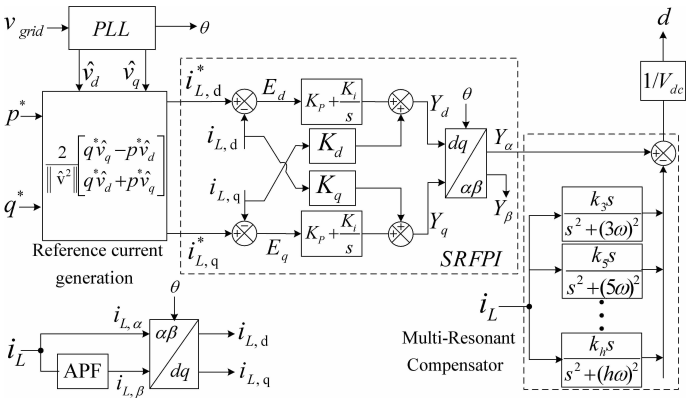

Fig. 3. Proposed control strategy

A. SRFPI Controller

Most of the current-controlled grid-connected inverters use either the inductor current or the output current as the control signal. It is shown that the system with inductor current feedback is more stable than that with output current feedback, especially when large variations of the grid impedance are expected [5]. Therefore, in this study, inductor current is chosen as the control signal.

As illustrated in Fig. 3, the DQ components of the inductor current, $i_{L,dq}$, are first generated by applying the APF and transformation matrix given in (2). These components are then compared with the reference currents $i^*_{L,dq}$, and the resultant errors, E_{dq}, are passed through two PI controllers to eliminate the tracking errors. In order to compensate the coupling between d and q axes, decoupling terms K_d and K_q are included.

$$K_d = (L_1 + L_2 + L_g)\omega \tag{14}$$

$$K_q = -(L_1 + L_2 + L_g)\omega \tag{15}$$

The output signals of the SRFPI controller, Y_{dq}, are transformed back into the stationary frame, where, naturally, only the real signal Y_α is fed to the grid-voltage disturbance compensator.

B. Grid Voltage Disturbance Compensator

It is well known that the grid voltage distortion introduces harmonic components in the grid current. The proposed SRFPI regulator attenuates current harmonics down to some extents. However, a specific harmonic compensator is required to further attenuate the harmonic content.

A multi-resonant harmonic compensator (HC) is proposed as a mean to further reduce the level of low-order current harmonic distortion (see Fig. 3). The transfer function of the harmonic compensator is given by:

$$HC(s) = \sum_{n=3,5,\ldots,h} \frac{k_n s}{s^2 + (n\omega)^2} \tag{16}$$

where n takes the values of 3, 5, . . . , h, where h is the highest current harmonic order to be attenuated, and k_n is the integrator gain for the nth-harmonic. In this paper, the highest current harmonic order of interest has been selected to be $h = 7$, as 3rd, 5th, and 7th harmonics are the most important harmonic components in the grid current.

C. Power Controller

There are two methods to control the output power: instantaneous and average power control. The instantaneous power control method leads to non-sinusoidal output current, when the grid voltage is distorted. Thus, to ensure high power quality injection, the average power control method is adopted in this study [3].

Using the power references p^* and q^* and filtered DQ components of grid voltage, $\hat{v}_{dq}$, and neglecting the filter capacitance, the inductor current references $i^*_{L,\,dq}$ can be calculated as follows:

$$\begin{bmatrix} i^*_{L,d} \\ i^*_{L,q} \end{bmatrix} = \frac{2}{\|\hat{v}^2\|} \begin{bmatrix} -\hat{v}_d & \hat{v}_q \\ \hat{v}_q & \hat{v}_d \end{bmatrix} \begin{bmatrix} p^* \\ q^* \end{bmatrix} \tag{17}$$

where $\left\|\hat{v}^2\right\| = \hat{v}_d^2 + \hat{v}_q^2$.

V. Single-Phase Equivalent of the SRFPI Regulator

Because of the utilization of the SRFPI controller in the current loop, the classical control techniques can not be applied. To overcome this problem, the single-phase equivalent of the SRFPI regulator is presented [4].

The transfer function $F(s)$ is the single-phase equivalent of the SRFPI regulator, and has a frequency response characteristic shown in Fig. 4.

$$F(s) = \left(k_p + \frac{k_i s^2 + 2\omega k_i s - k_i \omega^2}{s^3 + \omega s^2 + \omega^2 s + \omega^3}\right) \tag{18}$$

Notice, the transfer function $F(s)$ has a very high gain at the fundamental frequency. That is the reason why by using a SRFPI regulator, zero steady-state error at the fundamental frequency can be achieved.

Fig. 5 shows the single-phase equivalent of the proposed control system, in which the SRFPI regulator is replaced by F(s). $G_d(s) = e^{-T_d s}$ is the transfer function of the control processing delay, and $i_{ref} = i^*_{L,\,\alpha} = i^*_{L,\,d}\cos(\omega t) - i^*_{L,\,q}\sin(\omega t)$.

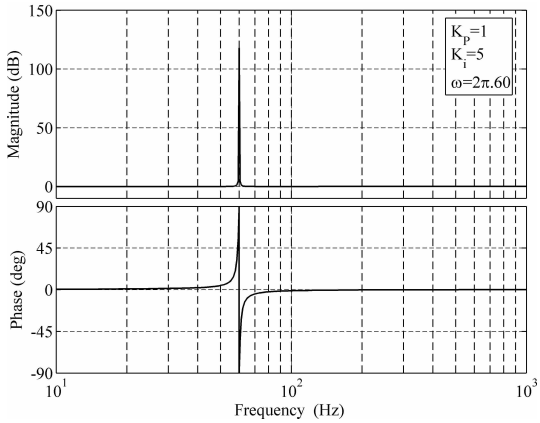

Fig. 4. Bode plot of transfer function $F(s)$

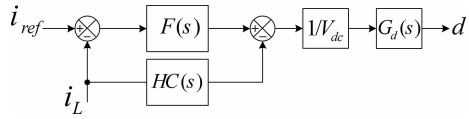

Fig. 5. Single-phase equivalent of proposed control system

From Fig. 5, the duty cycle dynamics can be written as follows:

$$d(s) = \{F(s)i_{ref} - [F(s) + HC(s)]\, i_L\}\, G_d(s)/V_{dc} \tag{19}$$

By substituting equations (19) into equation (7) and rearranging, the inverter side current dynamics can be expressed as:

$$i_L(s) = G_3(s) i_{L,\,ref}(s) - G_4(s) v_g(s) \tag{20}$$

where:

$$G_3(s) = \frac{G_1(s)F(s)G_d(s)/V_{dc}}{1 + T(s)} \tag{21}$$

$$G_4(s) = \frac{G_2(s)}{1 + T(s)} \tag{22}$$

The open loop gain $T(s)$ can be expressed as:

$$T(s) = G_1(s)(F(s) + HC(s))G_d(s)/V_{dc} \tag{23}$$

VI. Controller Parameters Design

The value of the proportional gain k_p determines the bandwidth, stability margin, and order of grid voltage harmonics that can be compensated without violating the stability limits [6]. Ideally, the bandwidth of closed loop system must be maximized by using a higher proportional gain k_p to obtain fast dynamic response, and high disturbance rejection capability. A high gain, however, degrades the control system stability and decreases the noise immunity of the system. Consequently, the choice of proportional gain k_p is a tradeoff between the stability margin and the bandwidth of the system.

In this paper, the design criterion of the proportional gain k_p is based on the crossover frequency selection of the open loop system. The analysis of the open-loop gain $T(s)$ using bode diagrams shows that the resistances of the LCL filter (r_1

and r_2), the grid resistance (r_g), the digital-implementation-related delay (T_d), and the integral and resonant terms have a negligible effect on the crossover frequency of the open loop system. Neglecting these terms, the open loop transfer function $T(s)$ can be rewritten as:

$$T(s) = k_p \frac{(L_2 + L_{g\omega})Cs^2 + 1}{L_1 C(L_2 + L_{g\omega})s^3 + (L1 + L2 + L_{g\omega})s} \quad (24)$$

Assume that the crossover frequency ω_{cros} is known, then the proportional gain k_p can be calculated as follows:

$$k_p = \left| \frac{L_1 C(L_2 + L_{g\omega})s^3 + (L1 + L2 + L_{g\omega})s}{(L_2 + L_{g\omega})Cs^2 + 1} \right|_{s=j\omega_{cros}} \quad (25)$$

To guarantee a sufficient stability margin, especially in weak grid condition, the crossover frequency must be greater than the frequency of highest grid current harmonic ($h\omega$) of interest [7], i.e. $\omega_{cros} > h\omega$. On the other hand, it must be low enough to avoid an excessive degradation of the phase margin. By considering a safety margin of $\omega_{saf} = 500\ rad/sec$ from the highest harmonic of interest at weak grid condition, the crossover frequency is determined to be $3140\ rad/sec$. By substituting $\omega_{cros} = 3140$ into (25) the proportional gain is calculated to be $k_p = 25.2$.

The integral term k_i and resonant terms k_n act to reduce the fundamental and low-order harmonic current errors. The values of these terms determine the bandwidth centered at the concerned frequencies, as shown in Fig. 6.

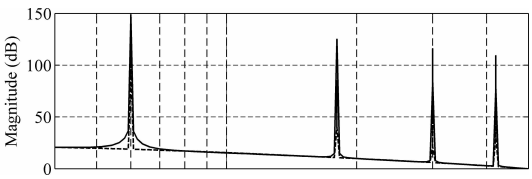

Fig. 6. Magnitude of open loop gain $T(s)$ for different values of integral and resonant terms (solid line: $k_i = k_n = 1000$, and dashed line: $k_i = k_n = 10$)

It should be noted that both SRFPI regulator and multi-resonant harmonic compensator are frequency dependent (see (16) and (18)), thus grid frequency fluctuations may degrade the performance of these regulators. Usually, the grid frequency is permitted to vary in a narrow band, typically $\pm 1Hz$. Thus, using the high integral and resonant terms, it is possible to reduce the negative effect of grid frequency fluctuations.

Due to the intricacy of the control system, simulation techniques have been used to determine the value of the integral and resonant terms. The selected values of the integral and resonant terms are summarized in Table II.

TABLE II
SELECTED VALUES OF INTEGRAL AND RESONANT TERMS

Symbol	k_i	k_3	k_5	k_7
Value	1000	500	500	500

Fig. 7 shows the bode diagram of the open loop gain $T(s)$, with k_p=25.2, $k_i = 1000$, $k_{3,5,7} = 500$, and the system parameters listed in Table I.

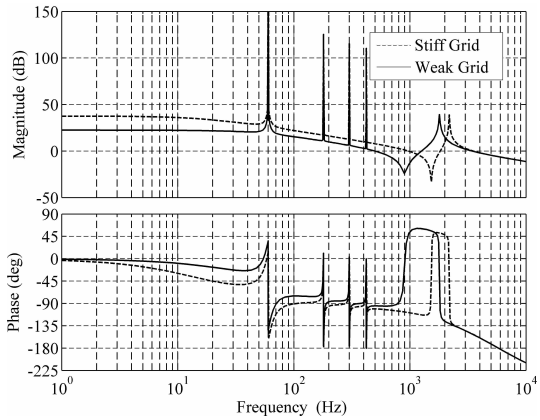

Fig. 7. bode diagram of open loop gain $T(s)$

From Fig. 7, the loop gain at the fundamental frequency ($|T(s)|_{@60Hz}$), the crossover frequency (ω_{cros}), the gain margin (GM), and the phase margin (PM) can be easily calculated. Table III shows the obtained results. These results demonstrate the excellent stability of the closed-loop system in both stiff and weak grid conditions.

TABLE III
OBTAINED RESULTS FOR DIFFERENT GRID CONDITIONS

Grid condition	GM	PM	ω_{cros}	$\lvert T(s)\rvert_{@60Hz}$
Stiff grid	6 dB	71°	6088 rad/sec	220 dB
Weak grid	6.03 dB	85°	3141 rad/sec	150 dB

VII. SIMULATION RESULTS

The performance of the proposed control strategy has been investigated using MATLAB/SIMULINK simulations. The simulations are carried out in weak grid condition. A complete set of results including transient response, and power control response are reported.

A. Current Control Performance

Fig. 8 shows the steady state performance of the current controller under weak grid condition. The grid voltage total harmonic distortion (THD) is about 10%. The d-axis current reference is set to $25A$, while the q-axis current reference is set to zero. As it can be seen, the reference tracking ability of the control system is very good, and the tracking error is very small. The harmonic spectrum of the output current is shown in Fig. 9.

Fig. 10 depicts the transient performance of the current controller for a step change in the q-axis current reference, I_q^*, from 0 to $25\,A$ at $t = 0.046\,s$. The d-axis current reference is set to zero. As it can be seen, the transient performance is very good, and the inductor current tracks its reference trajectory rapidly with near zero steady-state error and zero overshoot.

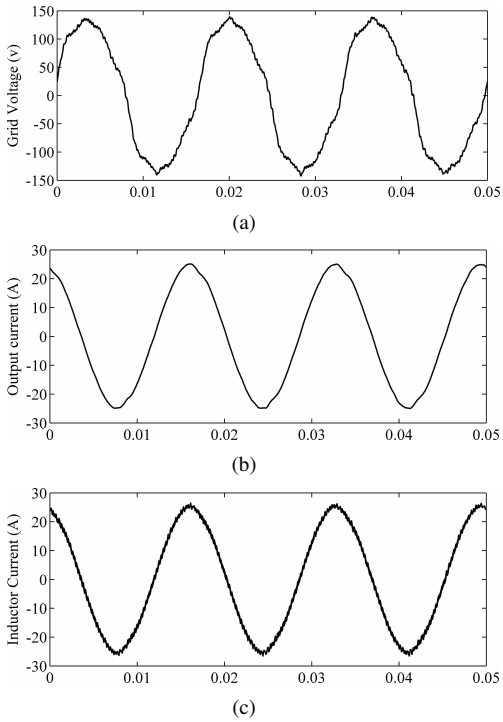

Fig. 8. Steady state performance of proposed controller.

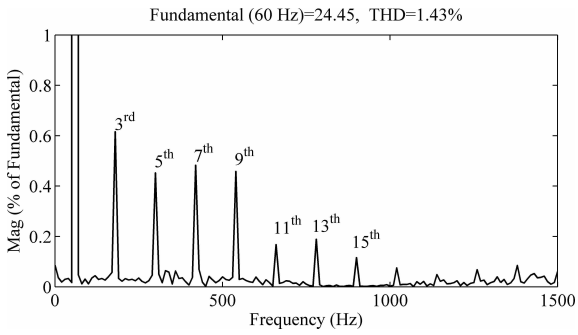

Fig. 9. Harmonic spectrum of output current

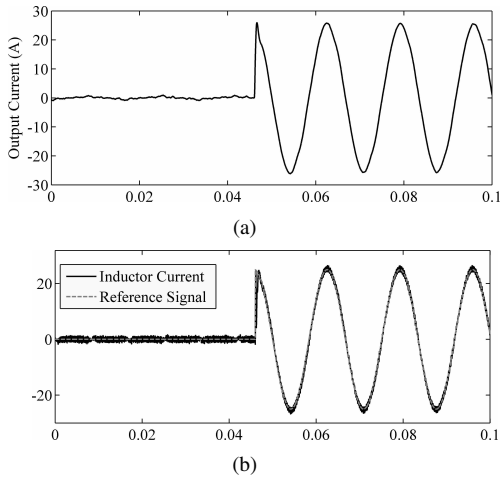

Fig. 10. Transient performance of current controller for a step jump in q-axis current reference.

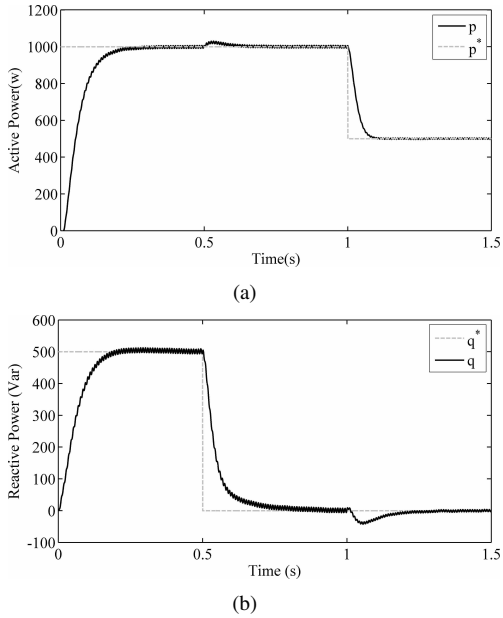

Fig. 11. Reference and actual values of active and reactive powers.

B. Power Control

In order to investigate the performance of the overall control system, step changes in the demanded active and reactive powers are given. The reactive power is dropped from 500 Var to 0 at $t = 0.5s$, and the active power command is dropped from $1000W$ to $500W$ at $t = 1s$. The output active and reactive powers of the system together with the reference values are shown in Fig. 11. It can be seen that the response to the change in command values is fast, and the control of the active and reactive power is decoupled. The small fluctuations, during step changes, are mainly due to the weak coupling between the direct and quadrature current control loops.

VIII. Conclusion

A synchronous reference frame PI (SRFPI) controller plus a multi-resonant harmonic compensator for single-phase grid-connected voltage source inverters has been presented in this paper. The essence of the proposed control strategy is to use a synchronous reference frame PI controller (SRFPI) to regulate the output current with zero steady state error, together with a multi-resonant harmonic compensator to provide an efficient attenuation of the grid voltage background harmonic distortion, and an average power controller to regulate the active and reactive power injection into the grid. Because of the use of the SRFPI controller in the current control loop, the classical control techniques can not be applied to evaluate the stability of the closed loop system. Thus, the single-phase equivalent of the SRFPI regulator was provided, which, significantly simplifies the controller design and stability analysis. A detailed design procedure with consideration of the practical implementation aspects has been presented and applied to the proposed control strategy. The performance

of the proposed control strategy has been investigated using MATLAB/SIMULINK simulations. The simulation results exhibit satisfactory steady state and transient performance, particularly under weak grid condition.

ACKNOWLEDGEMENT

This work was financially supported by an Islamic Azad University Research Grant.

REFERENCES

[1] G. Shen, D. Xu, L. Cao, and X. Zhu, "An improved control strategy for grid-connected voltage source inverters with an lcl filter," IEEE Trans. Power Electron., vol. 23, no. 4, pp. 18991906, July 2008.

[2] Y. A.-R. I. Mohamed, E. F. El-Saadany, and M. M. A. Salama, "Adaptive Grid-Voltage Sensorless Control Scheme for Inverter-Based Distributed Generation" IEEE Trans. Energy Convers., vol. 24, no. 3, pp. 683-694, Sep. 2009.

[3] Y. A. R. I. Mohamed and E. F. El-Saadany, "Adaptive discrete-time grid-voltage sensorless interfacing scheme for grid-connected DG-inverters based on neural-network identification and deadbeat current regulation," IEEE Trans. Power Electron., vol. 23, no. 1, pp. 302-321, Jan. 2008.

[4] S. Golestan, M. Monfared, J. M. Guerrero, and M. Joorabian, "A D-Q Synchronous Frame Controller for Single-Phase Inverters" 2nd Power Electrnics, Drive systems and Technologies Conference (PEDST 2011), Feb. 2011.

[5] T. Abeyasekera, C. M. Johnson, D. J. Atkinson, and M. Armstrong, "Suppression of line voltage related distortion in current controlled grid connected inverters," IEEE Trans. Power Electron., vol. 20, p. 1393, Nov. 2005.

[6] X. Yuan, W. Merk, H. Stemmler, and J. Allmeling, "Stationary-frame generalized integrators for current control of active power filters with zero steady-state error for current harmonics of concern under unbalanced and distorted operating conditions," IEEE Trans. Ind. Appl., vol. 38, no. 2, pp. 523-532, Mar./Apr. 2002. 2703-2709, Nov. 2008.

[7] M. Liserre, R. Teodorescu, and F. Blaabjerg, "Stability of photovoltaic and wind turbine grid-connected inverters for a large set of grid impedance values," IEEE Trans. Power Electron., vol. 21, no. 1, pp. 263-272, Jan. 2006.